Available online at www.sciencedirect.com
ScienceDirect
Catalysis Today 122 (2007) 378–385
CATALYSIS TODAY
www.elsevier.com/locate/cattod

Synergistic activity of gold-platinum alloy nanoparticle catalysts

Derrick Mott, Jin Luo, Peter N. Njoki, Yan Lin, Lingyan Wang, Chuan-Jian Zhong *

Department of Chemistry, State University of New York at Binghamton, Binghamton, NY 13902, USA

Available online 14 January 2007

Abstract

The understanding of the composition–activity relationship is essential for the exploitation of the synergistic properties of multimetallic nanoparticles in catalytic reactions. This paper focuses on the discussion of findings from the investigation of bimetallic gold-platinum (AuPt) nanoparticles of different compositions. Infrared spectroscopic data for CO adsorption on silica-supported AuPt nanoparticles reveal that the surface binding sites are dependent on the bimetallic composition. The analysis of this dependence further led to the conclusion that the relative Au-atop and Pt-atop sites for the linear CO adsorption on the nanoparticle surface are not only correlated with the bimetallic composition, but also with the electronic effect as a result of the d-band shift of Pt in the bimetallic nanocrystals, which is the first demonstration of the nanoscale core–surface property correlation for the bimetallic nanoparticles over a wide range of bimetallic composition. A further examination of the electrocatalysis data for methanol oxidation reaction on carbon-supported AuPt nanoparticle catalysts reveal important insights into the participation of CO or OH adsorption on Au sites and the catalytic activity of Pt in the AuPt alloys with relatively high Au concentration. Implications of these findings to synergistic correlation of the bifunctional activity of the bimetallic nanoparticle catalysts with the bimetallic composition are also discussed.

Keywords: Nanoparticles; AuPt alloys; Pt-atop sites

1. Introduction

Despite the intensive research into the catalytic activity of gold in a restricted nanoscale size range [1], the catalytic origin of nanosized gold and gold-based bimetallic catalysts remains elusive. One of the main problems is the lack in understanding of the nanoscale core–surface property correlation. Gold-platinum nanoparticles of 2–5 nm diameter presents an intriguing system for delineating the correlation in view of recent ability in synthesizing AuPt nanoparticles in a wide range of bimetallic composition [2]. Is the AuPt nanocrystal core alloyed or phase-segregated? How are the surface binding properties correlated with the nanoscale bimetallic properties? The answers to these questions have important implications not only to the exploitation of catalytic activity of the nanoscale bimetallic catalysts, but also to the general exploration of the surface or interfacial reactivities of bimetallic or multimetallic nanoparticles. XRD studies [2] revealed alloy properties for the nanocrystal core which is in contrast to the miscibility gap known for the bulk counterparts [3]. An infrared spectroscopic study of the adsorption of CO on the nanoparticles can effectively address the surface binding properties because its stretching frequency is highly sensitive to the surface binding sites [4], as widely reported for oxide-supported gold, platinum, gold-platinum and other bimetallic catalysts prepared by vapor deposition [5], cation-exchange, insipient wetness impregnation [6] and dendrimer or cluster based methods [6,7].

The understanding of the bimetallic nanocrystal phase and surface binding properties is essential to address some of the major problems in direct methanol oxidation fuel cells, such as poor activity of the anode catalysts, the ‘‘methanol cross-over’’ to the cathode electrode [8,9], and the poisoning of Pt catalysts by CO-like intermediate species [10–12]. The exploration of nanoscale gold-based bimetallic materials could potentially provide a synergistic catalytic effect by minimizing or eliminating the poisoning problem. For example, gold-platinum (AuPt) nanoparticles could provide a synergistic catalytic effect that involves the suppression of adsorbed poisonous species and a change in electronic band structure to modify the strength of the surface adsorption. With such a bimetallic system, one could explore the viability of using Pt as the main dehydrogenation sites, and Au together with Pt to

* Corresponding author. Tel.: +1 607 777 4605.
E-mail address: cjzhong@binghamton.edu (C.-J. Zhong).

0920-5861/$ – see front matter © 2007 Elsevier B.V. All rights reserved.
doi:10.1016/j.cattod.2007.01.007

speed up the removal of poisonous species. The decrease in activation energy to facilitate oxidative desorption or suppress CO adsorption was previously considered to lead to sufficiently high adsorptivity to support catalytic oxidation in alkaline electrolytes [13–16]. A recent study [6] showed that catalysts prepared by impregnation from Pt and Au precursors are similar to those of monometallic Pt catalysts, suggesting that the presence of Au did not affect the catalytic performance of Pt in any significant way. This was attributed to phase-segregation of the two metals due to their miscibility gap. Recent density functional theory (DFT) calculations [17] have indicated that the d-band shift for Pt in a Pt-Au alloy on Au(1 1 1) differs from that for a Pt-Au alloy on Pt(1 1 1). A stronger bonding of CO to the first layer of Pt on Au(1 1 1) exists compared with the binding of CO on clean Pt. The Au substrate surprisingly increases the Pt overlayer reactivity. The modeling suggests that the change in the CO binding energy is proportional to the shift of the d-band center of the metal overlayer. The adsorption of CO showed an increased binding energy in comparison with Pt(1 1 1), due to the larger lattice constant of Au, leading to an expansion of Pt. The shift of d-band depends strongly on Au coverage. The CO desorption temperature from an AuPt alloy was shown to depend linearly on Au coverage [18]. The understanding of how such a d-band shift applies for AuPt alloy nanoparticles has important implications to the design of bimetallic nanoparticle catalysts.

While the electrocatalytic activity of the bimetallic catalysts for methanol oxidation reaction (MOR) has been demonstrated for AuPt nanoparticles prepared by molecular-capping based chemical synthesis and subsequent assembly on carbon black support and thermal activation treatment [19,20], the question of how the bimetallic nanocrystal and surface alloy properties are related to the surface binding and catalytic activities remain unanswered. In view of the finding that the alloy properties of the bimetallic AuPt nanoparticles are in sharp contrast to the bimetallic miscibility gap known for the bulk counterparts in a wide composition range (10–80% Au), there is a clear need to assess the surface binding and the electrocatalytic properties of the catalysts with different bimetallic compositions. We report herein the recent results of an investigation of the CO adsorption and the electrocatalytic MOR activities of AuPt nanoparticle catalysts with different bimetallic composition. The aim is to gain insights into the correlation between the nanoscale core and surface properties over a wide range of bimetallic composition [20,21].

2. Experimental

2.1. Chemicals

Decanethiol (DT, 96%), oleylamine (OAM, 70%), hydrogen tetrachloroaurate ($HAuCl_4$, 99%), tetraoctylammonium bromide (TOABr, 99%), hydrogen hexachloroplatinate (IV) ($H_2PtCl_6{\cdot}xH_2O$, 99.995%), sodium borohydride ($NaBH_4$, 99%), methanol (99.9%), ethanol (99.9%), silica gel (syloid 74) and Nafion (5 wt%) were purchased from Aldrich and used as received. Other chemicals included hexane (99.9%) and toluene (99.8%) from Fisher. Carbon black (Vulcan XC-72) was obtained from Cabot. Water was purified with a Millipore Milli-Q water system.

2.2. Synthesis of nanoparticles

The Au, Pt and AuPt catalysts were prepared by a combination of two protocols. The first involved a modified two-phase synthesis [2,22] of nanoparticles of ~2 nm core sizes with different compositions (Au_mPt_{100-m}) capped with a mixed monolayer of decanethiolate and oleylamine (as-synthesized nanoparticles) [23,24]. The control of AuPt composition in the range of 10–90% Au with 2–4 nm core sizes and high monodispersity ($< \pm 0.5$ nm) was achieved by manipulating the precursor feed ratio. The second protocol involved assembly of the as-synthesized nanoparticles on different supports (e.g., carbon (C) and silica (SiO_2)) [21], followed by subsequent thermal treatment under controlled temperature and atmosphere [20]. The thermal treatment involved heating the catalyst at 300 °C under 20% O_2 followed by treatment at 400–600 °C under 15% H_2. It has been found that the temperature range of 400–500 °C is the most appropriate thermal treatment condition for both the electrocatalytic and the alloying properties [2]. The actual loading ranged from 2.5 to 5.4% by mass for typical samples. The silica-loaded nanoparticles were thermally treated under controlled atmosphere and temperature, including shell removal under 300 °C with 20% O_2/N_2 for 1 h and calcination under 400 °C with 15% H_2/N_2 for 2 h. Several nanoparticle samples were synthesized and subsequently studied in this paper, which are listed in Table 1.

2.3. Preparation of catalysts on electrodes

Glassy carbon (GC) disks (geometric area: 0.07 cm^2) were polished with 0.03 μm Al_2O_3 powders. The geometric area of the substrate electrode (glassy carbon), not the surface area of the catalyst itself, provides a measure of the loading of catalyst on the electrode surface. A typical suspension of the catalysts was prepared by adding 1 mg catalyst (AuPt/C) to 1 mL of 0.25% Nafion solution, and sonicating for 15 min. The suspension was stable for several days. The suspension was then quantitatively transferred to the surface of the polished GC disk. The electrodes were dried overnight at room temperature.

Table 1
Compositions of AuPt nanoparticles studied throughout

Sample	Bimetallic composition (atomic %)	
	Au (%)	Pt (%)
Au	100	0
$Au_{96}Pt_4$	96	4
$Au_{82}Pt_{18}$	82	18
$Au_{72}Pt_{28}$	72	28
$Au_{65}Pt_{35}$	65	35
$Au_{56}Pt_{44}$	56	44
$Au_{43}Pt_{57}$	43	57
$Au_{35}Pt_{65}$	35	65
Pt	0	100

2.4. Measurements

Direct current plasma-atomic emission spectroscopy (DCP-AES) was employed to analyze the composition of the as-synthesized bimetallic nanoparticles and the thermally treated nanoparticles on supports (carbon black or SiO_2) using an ARL Fisons SS-7 DCP-AES instrument, the measurements were made on emission peaks at 267.59 and 265.95 nm for Au and Pt, respectively. The nanoparticle samples were dissolved in concentrated aqua regia, and then diluted to concentrations in the range of 1–50 ppm for analysis. Calibration curves were made from dissolved standards with concentrations from 0 to 50 ppm in the same acid matrix as the unknowns. Standards and unknowns were analyzed 10 times each for 3 s counts. Instrument reproducibility, for concentrations greater than 100 times the detection limit, results in $< \pm 2\%$ error. For example, the DCP analysis of the bimetallic nanoparticles synthesized under the above conditions yielded an atomic composition of 35% Au and 65% Pt. The nanoparticles of this composition is denoted as $Au_{35}Pt_{65}$.

Transmission electron microscopy (TEM) was performed on a Hitachi H-7000 electron microscope (100 kV). For TEM measurements, samples were suspended in hexane solution and were cast by dropping the nanoparticle solution onto a carbon-coated copper grid followed by solvent evaporation in air at room temperature.

X-ray powder diffraction (XRD) data were collected on a Philips X'Pert diffractometer using Cu Kα radiation (λ = 1.5418 Å). The measurements were done in reflection geometry and the diffraction (Bragg) angles 2θ were scanned at a step of 0.025°. Each data point was measured for at least 20 s and several scans were taken of each sample.

Fourier transform infrared spectra (FT-IR) were acquired on a Nicolet Magna 760 spectrometer. The sample cell for the FT-IR measurement consists of a glass tube with two windows and two gas-flow valves on the side, which allowed for purging with nitrogen and CO. The thermally treated catalysts were ground into fine powders and pressed into a pellet, which was mounted inside the glass tube on a NaCl window plate. Sixty-four scans were collected for each spectrum with a resolution of 4 cm^{-1}. Spectra were acquired at room temperature by first purging the chamber with nitrogen and then taking a background spectrum. The chamber was then purged with ~4% CO in nitrogen (for 10 min), and a spectrum was taken. By subtracting the spectrum of the gas-phase CO (2171 and 2119 cm^{-1}) generated in a separate measurement under the same conditions without the catalyst, the resulting spectrum was obtained that corresponded to the CO molecules adsorbed on the catalyst. In the present study, we focused on the relative shift of the CO adsorption bands by keeping the same preparation and measurement conditions. The gas-phase CO can be purged away in less than 5 min. The resolution did not constitute an issue to affect the data assessment. All spectra were baseline corrected and water subtracted.

The cyclic voltammetry (CV) measurements were performed using a microcomputer-controlled electrochemical analyzer (CHI600a, CH Instruments), using three-electrode electrochemical cells at room temperature. All electrolytic solutions were de-aerated with high purity argon or nitrogen before the measurement. The potentials are given with respect to the reference electrode of Ag/AgCl saturated KCl.

3. Results and discussion

The discussion of the experimental results is divided into three sections. In the first section, the morphological, composition and structural properties of the bimetallic alloy nanoparticle catalysts are described. The second section discusses the results of an investigation of the CO adsorption using FT-IR. The results allowed us to establish the correlation between the bimetallic composition in the nanoparticles and the strength of CO adsorption of the bimetallic catalysts. The third section describes the results from the characterization of the electrocatalytic MOR activity.

3.1. Morphological, composition and structural properties

Au_mPt_{100-m} nanoparticles with different atomic compositions ranging from $m \approx 10$ to 90% Au have been synthesized by the method described in Section 2. Varying the feeding ratio of the metal precursors used in the synthesis controlled the bimetallic composition of the nanoparticles. The average sizes of the as-synthesized particles determined from TEM data are 2.2 ± 0.2 nm for Au, 4.8 ± 0.8 nm for Pt and 1.8 ± 0.6 nm for $Au_{82}Pt_{18}$ nanoparticles [2]. While the average sizes were slightly increased for the nanoparticles on SiO_2 after thermal treatment (e.g., 3.8 ± 0.7 nm for Au/SiO_2 and 3.3 ± 0.4 for $Au_{82}Pt_{18}/SiO_2$) in comparison with the as-synthesized particles (likely due to sintering effect), they displayed high monodispersity. Each sample shown in Table 1 was analyzed using TEM for size and morphology. It was found that all samples had similar sizes. Fig. 1A shows a typical TEM micrograph for the carbon-supported AuPt nanoparticles after thermal treatment (example: $Au_{82}Pt_{18}$). The high-resolution TEM image (Fig. 1A, bottom inset) indicates that the thermally treated nanoparticles exhibit a highly crystalline morphology. As demonstrated in our earlier report [25], there are two important pieces of evidence supporting the effective removal of the capping monolayers from the nanoparticles by the thermal-treatment process. First, the vibrational bands characteristic of the capping molecules in the C–H stretching region ($\nu_a(CH_3)$, 2955 cm^{-1}; $\nu_s(CH_3)$, 2872 cm^{-1}; $\nu_a(CH_2)$, 2917 cm^{-1}; $\nu_s(CH_2)$, 2848 cm^{-1}) were not detected by FT-IR. Secondly, XPS analysis showed that the bands associated with sulfur species ($S(2p_{1/2})$, 163.8 eV; $S(2p_{3/2})$, 162.5 eV) were absent after the thermal treatment.

A close examination of the XRD data for AuPt nanoparticles over a wide range of bimetallic composition [2] provides important information for assessing the phase properties of these bimetallic nanomaterials. In contrast to the bulk Au-Pt counterparts which display a miscibility gap at 20–90% Au [3], as shown by the open circle data points and lines in Fig. 1B, the lattice parameters of the bimetallic nanoparticles, as shown by the half filled circle data points and lines, were found to scale linearly with Pt%. Such a relationship follows a Vegard's type

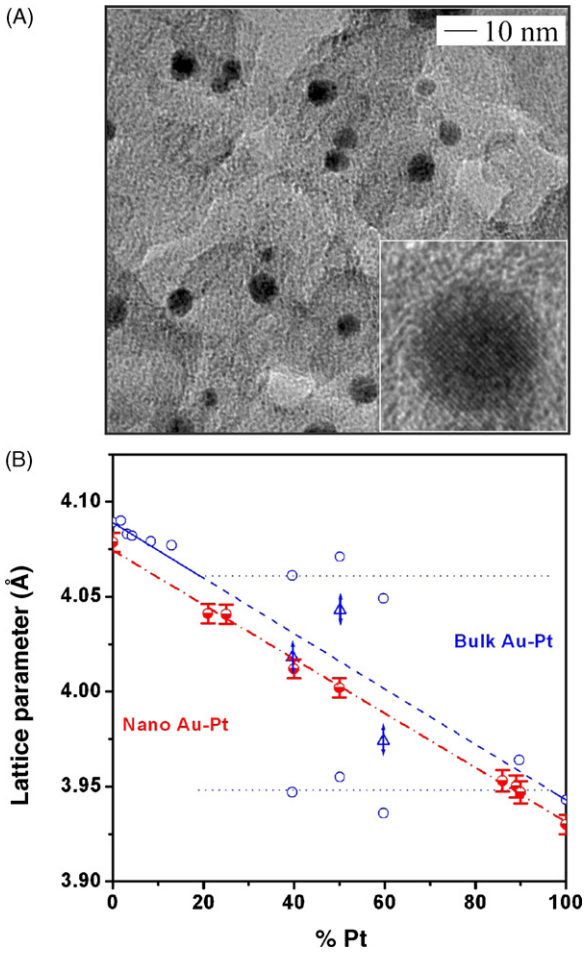

Fig. 1. (A) TEM and HRTEM of $Au_{82}Pt_{18}$/C. (B) The lattice parameters vs. Pt% for AuPt nanoparticles (◒), part of the data reported recently [2], and for bulk AuPt [3] (○) (triangular points represent a frozen state for bulk metals).

law typically observed with binary metallic alloys, demonstrating the alloy properties for the bimetallic AuPt nanoparticles [2]. The XRD pattern for $Au_{52}Pt_{48}$ synthesized using the different protocol also showed alloy feature [26].

The thermal treatment of the catalysts is also believed to influence the core and the surface crystallinity properties of the nanocrystals. As stated in Section 1 on our recent XRD study [2], the carbon-supported AuPt nanoparticles treated at 500 °C exhibit single-phase characteristics as demonstrated by the linear relationship between the lattice parameters and the composition. While the diffraction patterns are characteristic of the fcc-type lattice, there are subtle differences in peak shape, width and position. The lattice parameters were determined for each AuPt sample by carefully determining the positions of the Bragg peaks in the diffraction patterns. The Bragg peaks (2θ) for the (1 1 1) plane are found at 38.6 or 38.3 for 400 or 500 °C for treated $Au_{82}Pt_{18}$ samples, respectively [22]. It seems that the relative changes in peak width and symmetry are more significant than that in peak position, which likely suggests a higher degree of crystallinity for the catalysts treated at 500 °C in comparison with that at 400 °C. There was also a slight increase in particle size, and the estimate from the XRD peak widths (from the (1 1 1) peak) yielded 4.2 (±0.5 nm) and 5.0 nm (±0.5 nm) after the treatment after 400 and 500 °C, respectively, which are close to those determined from TEM data [22]. Upon further increasing the treatment temperature to higher than ~650 °C, experiments revealed indications of phase-segregation and larger particle sizes. In addition, the values for the lattice parameter of the nanoscale AuPt are all smaller than those for the bulk AuPt. This intriguing phenomenon suggests that nanoparticles have smaller inter-atomic distances than those for the bulk counterparts [27]. To our knowledge, this is the first example demonstrating that the nanoscale AuPt nanoparticles not only have single-phase character but also small inter-atomic distances in the entire bimetallic composition range, both which are in sharp contrast to those known for their bulk counterparts.

3.2. CO adsorption

A comparison among infrared spectra for CO adsorption on AuPt nanoparticles over a wide range of bimetallic composition provides important information for assessing the surface binding properties of these bimetallic nanomaterials. All of the samples here were immediately analyzed after removing them from the tube furnace after the thermal treatment to minimize poisoning and deactivation effects of adsorbed species. We have also performed heating experiments, but we did not observe any water effects for samples prepared this way. In addition, we observed no indication of additional adsorbed species in our analysis. There was no indication of CO_2 in the spectra of these samples. By comparing CO spectra for Au/SiO_2, Pt/SiO_2, physical mixtures of Au/SiO_2 and Pt/SiO_2, and an $Au_{72}Pt_{28}$/SiO_2 alloy, the CO bands for the bimetallic alloy catalyst are detected at 2115 and 2066 cm^{-1}, which are distinctively different from the single band feature at 2115-cm^{-1} for CO linearly adsorbed on atop sites of Au [4,28–30], and the single band feature at 2096-cm^{-1} for CO on atop sites for Pt [4,31]. The observation of single bands for CO adsorbed on both Au and Pt sites is in agreement with observations reported in two previous studies [6,7] for gold-platinum bimetallic catalysts synthesized by other methods. For example, for AuPt prepared by a 1:1-feeding ratio in a dendrimer-based synthesis [7], the observed 2113-cm^{-1} band was attributed to adsorption on Au sites though the band for CO on monometallic gold was not detected, and a 2063-cm^{-1} band was attributed to CO on Pt sites which was explained due to dilution and dipole coupling effects. For the cluster-derived AuPt bimetallic catalyst [6], the observed 2117-cm^{-1} band was similarly attributed to CO adsorbed to Au sites and the observed 2064-cm^{-1} band was assigned to CO at Pt sites due to an electronic effect caused by the incorporation of Au to the bimetallic catalyst and not the dipolar coupling effect as supported by ^{13}CO data.

Fig. 2 shows a representative set of FT-IR spectra comparing CO adsorption on AuPt/SiO_2 with a wide range of bimetallic compositions. Two most important features can be observed from the spectral evolution as a function of bimetallic composition. First, the 2115-cm^{-1} band observed for Au/SiO_2 (a) displays a clear trend of diminishing absorbance as Pt

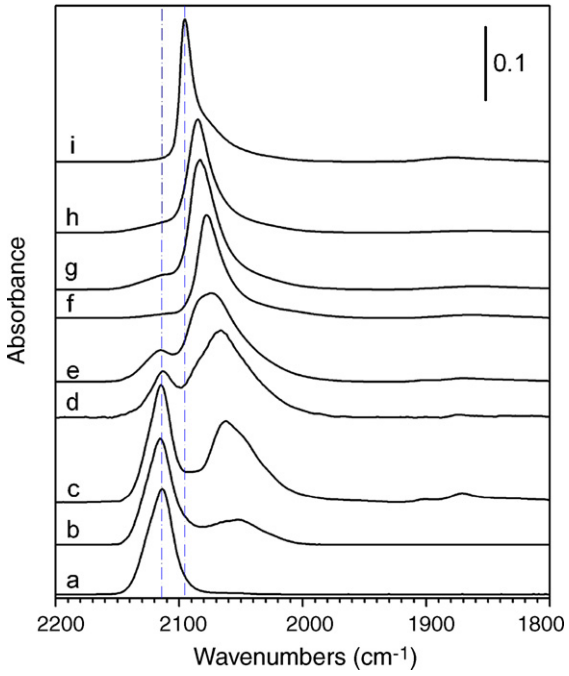

Fig. 2. Comparison of FT-IR spectra of CO adsorption on SiO_2-supported AuPt nanoparticle catalysts of different composition: (a) Au/SiO_2, (b) $Au_{96}Pt_4/SiO_2$, (c) $Au_{82}Pt_{18}/SiO_2$, (d) $Au_{72}Pt_{28}/SiO_2$, (e) $Au_{65}Pt_{35}/SiO_2$, (f) $Au_{56}Pt_{44}/SiO_2$, (g) $Au_{43}Pt_{57}/SiO_2$, (h) $Au_{35}Pt_{65}/SiO_2$ and (i) Pt/SiO_2.

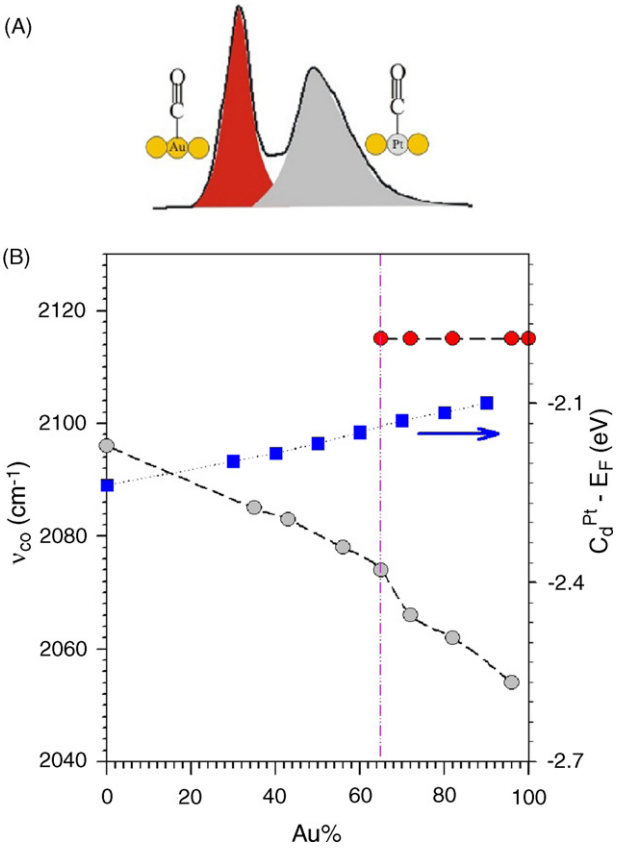

Fig. 3. (A) Schematic illustration of the band assignment for CO adsorbed to Au-atop site surrounded by Au atoms, and Pt-atop site surrounded by Au atoms for a AuPt alloy surface. (B) Plots of the wavelength for Au-atop (red circle, at top) and Pt-atop (gray circle, at bottom) CO bands vs. the composition of Au in the alloy AuPt nanoparticles, along with the calculated trend in the d-band shift for Pt atoms in AuPt alloy on a Au(1 1 1) based on calculation results in ref. [17] (blue filled square). (For interpretation of the references to color in this figure legend, the reader is referred to the web version of the article.)

concentration increases in the bimetallic catalysts. It is very interesting that this band becomes insignificant or even absent at $> \sim 45\%$ Pt. Secondly, the lower wavenumber CO band ($\sim$2050 cm^{-1}) shows a clear trend of shift towards that for the Pt-atop CO band observed for Pt/SiO_2 (i) as Pt concentration increases. This trend is shown in Fig. 3. For higher concentrations of Au, this band is strong and broad. Such a dependence of the CO bands on the bimetallic concentration is remarkable, and is to our knowledge observed for the first time. The higher wavenumber band (2115 cm^{-1}) is attributed to CO adsorption on Au-atop sites in a Au-rich surface environment, whereas the lower wavenumber band and its composition-dependent shift reflect an electronic effect of the surface Pt-atop sites alloyed in the bimetallic nanocrystal. The fact that the disappearance of the Au-atop CO band at $> \sim 45\%$ Pt is accompanied by a gradual shift of the Pt-atop CO band is indicative of a unique synergistic surface property in which the Pt-atop CO adsorption is greatly favored over the Au-atop CO adsorption. The observation of heightened CO band intensity for some samples could be a result of the unique activity of the catalyst, which is part of our on-going investigation. To understand this preference, we must understand how Au atoms surrounding Pt atoms produce an electronic effect on the binding properties of CO on Pt.

The understanding of the electronic effect is based on the correlation between the spectral features and findings from a previous DFT calculation on the d-band of Pt atoms in bimetallic AuPt surfaces [17]. The DFT calculation showed that the d-band center of Pt atoms increases with Au concentration in the AuPt alloy on a Au(1 1 1) or Pt(1 1 1) substrate. For an AuPt alloy on Au(1 1 1), the d-band center of Pt atoms was found to show an increase from 0 to 65–70% Au, after which a slight decrease was observed. For a AuPt alloy on Pt(1 1 1), the d-band center of Pt atoms is found to increase almost linearly with the concentration of Au. Both were supported by experimental data in which the adsorption of CO showed an increased binding energy in comparison with Pt(1 1 1), due to the larger lattice constant of Au, leading to an expansion of Pt [17,18]. Since the theoretical data for nanocrystal alloys are not yet available, the average d-band shift for Pt atoms from these two sets of DFT calculation results is included in Fig. 3 to illustrate the general trend. Since the DFT results provide information on the Pt surface binding properties, let us consider that the maximum concentration of Pt atoms on the surface in which each Pt atom is completely surrounded by Au atoms. The Pt concentration is 33% for $\sqrt{3} \times \sqrt{3}$ (1 1 1) or 50% for 2×2 (1 0 0) for a single layer bimetallic surface, and 25% (1 1 1) or 16% (1 0 0) for a multi-layer structure [32]. An average of these values would yield 30–33%, which coincides closely with the observed maximum of the d-band for Pt atoms in an AuPt alloy on Au(1 1 1) [17]. Interestingly, a subtle transition for the lower-wavenumber band, i.e., from a relatively broad band

feature to a narrow band feature that resembles that of the Pt-atop CO band is observed to occur at ~65% Au, below which the Au-atop CO band basically disappeared. There exists a stronger electron donation to the CO band by a Pt-atop site surrounded by Au atoms in the bimetallic alloy surface than that from the monometallic Pt surface as a consequence of the upshift in d-band center of Pt atoms surrounded by Au atoms, which explains the preference of Pt-atop CO over the Au-atop CO adsorption. The observed decrease of the Pt-atop CO band frequency with increasing Au concentration is clearly in agreement with the d-band theory for the bimetallic system [17]. Note that the observed wavelength region of 2050–2080 cm^{-1} is quite close to those found recently based on DFT calculations of CO adsorption on AuPt clusters (2030 and 2070 cm^{-1}) depending on the binding site (Pt or Au) [33,34].

It is important to note that the complete disappearance of the Au-CO band for samples with a concentration below 65% Au does not necessarily imply the absence of Au on the surface of the nanoparticles; it implies rather the preferential Pt-atop CO adsorption over Au-atop CO adsorption, which is supported by the DFT calculation results [17]. This is an important finding, in contrast to the linear trend observed for the lattice parameter of the bimetallic alloy nanoparticles of different composition as evidenced by the XRD data.

3.3. Electrocatalytic MOR activity

As an initial step to determine the electrocatalytic MOR activity, the presence of Pt or Au on the surface of AuPt nanoparticle catalysts was first assessed by CV measurements of the catalysts loaded on glassy carbon electrodes in acidic or alkaline solution. In comparison with the redox waves for the monometallic Au and Pt catalysts (in 0.5 M KOH) which exhibit redox waves at −0.4 to 0.0 V for Pt and 0.0–0.4 V for Au [19], the detection of the redox waves corresponding to Au and Pt in the bimetallic $Au_{72}Pt_{28}$/C and $Au_{35}Pt_{65}$/C catalysts (Fig. 4A) demonstrate the presence of a bimetallic surface composition on the catalysts. This is consistent with the bimetallic nanoparticle core composition.

In the absence of methanol, the catalysts exhibit redox waves corresponding to gold and gold oxide on the surface. The gold oxidation wave was found at 0.3 V whereas the reduction wave was around 0.06–0.07 V for both catalysts. There seems to be a subtle difference in the redox current, which is perhaps suggestive of the surface composition difference. The AuPt/C shows a methanol oxidation wave at around −0.15 V (Fig. 4B). The methanol oxidation activity was also found to be dependent on both composition and treatment temperature. Furthermore, a smaller anodic wave is observed at −20 mV on the reverse sweep for these AuPt/C catalysts, which is attributed to oxidation of methanol on re-activated catalyst surface [35].

The catalytic modification of the bimetallic composition is in fact further reflected by the remarkable difference of the voltammetric characteristic observed in the reverse scan, especially in the alkaline electrolyte. For Pt/C, the reverse wave for alkaline electrolyte occurs at a potential less positive than the forward wave by ~200 mV. In contrast, the reverse wave for

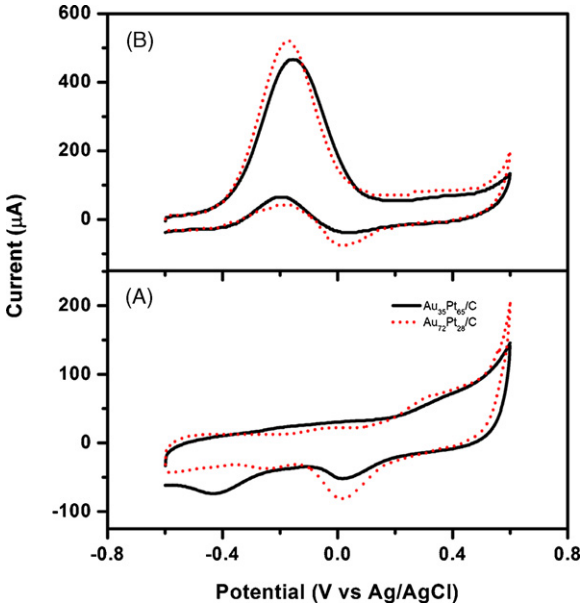

Fig. 4. CV curves of the carbon-supported nanoparticles, $Au_{72}Pt_{28}$/C (dashed lines) and $Au_{35}Pt_{65}$/C (solid lines) catalysts (metal loading: 20%), on a glassy carbon electrode in 0.5 M KOH without (A) and with (B) 0.5 M methanol. Scan rate: 50 mV/s (GC electrode area: 0.07 cm^2).

AuPt/C occurs at a potential which differs from the potential for the wave in the forward sweep by only ~20 mV. The relative peak current of the reverse/forward wave is also found to be dependent on Au% in the bimetallic nanoparticle. The oxides formed on the catalyst surface at the potential beyond the anodic peak potential in the positive sweep are reduced in the reverse sweep [35]. Poisonous CO species formed on the Pt surface can also be removed in the reverse sweep. The observation of the more positive potential for the reverse wave likely reflects the bimetallic effect on the re-activation of the catalyst surface after the anodic sweep. The re-activation of the surface catalytic sites after the anodic sweep is likely modified by the presence of Au in the catalyst, which leads to a shift in the peak potential of the reverse wave to a more positive potential (by ~200 mV) for AuPt/C than for Pt/C.

The correlation between the composition and the electrocatalytic activity for the above catalysts is assessed by analyzing the mass activity (i.e., the peak current density per unit total mass of metals) and the kinetic parameters (Tafel slope). Fig. 5 summarizes a representative set of results showing the dependence of MOR mass activity on the bimetallic composition. The dash lines show the general trend for the entire composition range of AuPt alloy nanoparticles. One of the significant findings is that the mass activity for the alkaline condition appears to exhibit a maximum around the composition of 65–85% Au, which is remarkably close to the composition range (~65%Au) observed for the transition of the band features (see Fig. 3). While the presence of Au in Pt increases the lattice distance of Pt, the higher electronegativity of Au than Pt could cause an increase of the amount of change being transferred from Pt to Au, which was in fact supported by high-resolution XPS data showing Au $4f_{7/2}$ binding energy 83.32 eV for Au/Pt and 83.87 eV bulk-like Au atoms [36], and

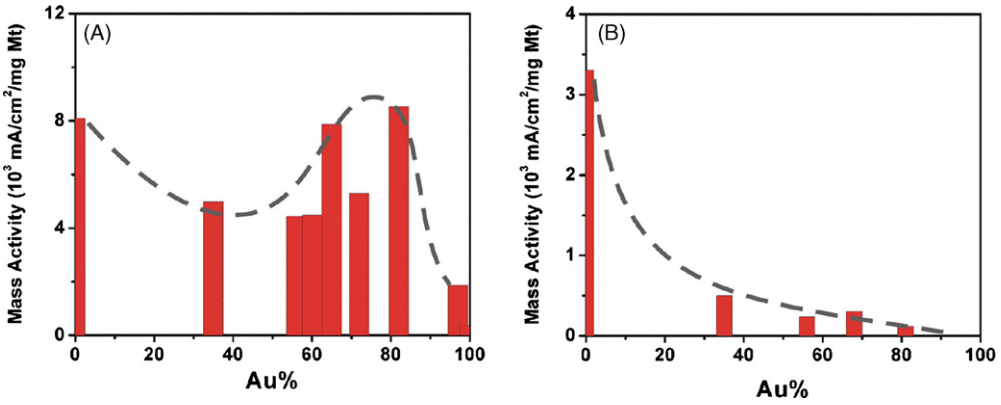

Fig. 5. (A) MOR mass activities vs. bimetallic composition for AuPt/C in 0.5 M KOH (left) and in 0.5 M H_2SO_4 (B) with 0.5 M MeOH (based on maximum current density in voltammetric curve at 50 mV/s) (dash line (not fitting) illustrates the general trend). (Mt: total metal loading of Au and Pt).

consequently, the increase of the d-orbital vacancy in the AuPt. The composition was found to significantly modify the electrocatalytic properties of both Au and Pt. The finding that the mass activity in the alkaline electrolyte exhibits a maximum around 65–85% Au is in contrast to the small and gradual increase from no activity of Au to high activity of Pt in the acidic electrolyte. The variation of Tafel slope appears to be relatively small (∼120 mV/dec). The display of the maximum mass activity for AuPt/C catalysts comparable or higher than that for Pt/C catalyst in the alkaline electrolyte is remarkable in view of the fact that only 15–35% Pt was present in the catalyst.

To understand the origin, recent modeling results based on a DFT calculation for CO adsorption on small clusters of AuPt [17,34] are considered. The modeling results showed that the CO adsorption energy increases with Pt% which maximize at ∼30% Pt for CO adsorption on Au atoms, and increases with Pt% for CO adsorption on Pt atoms for all compositions. This is important because it implies that gold atoms surrounding Pt atoms in the AuPt alloy with a relatively high percentage of Au may have played an important role in either removing the intermediate CO-like species or providing oxygenated species in the methanol oxidation process. This assessment is consistent with the known facts that the nanoscale Au is catalytically highly active for CO oxidation [1,37,38], and Au is known to be capable of producing surface oxygenated species in basic electrolytes [39,40].

We believe that a bifunctional electrocatalytic property may be operative for the bimetallic catalysts in the alkaline electrolyte. The similarity of the mass activity for the bimetallic catalyst with 65–85% Au to those for pure Pt catalyst is suggestive of the participation of Au in the catalytic reaction of Pt. The alloy character for both the surface and the core of the AuPt/C catalysts is supported by XRD data for the phase properties and FT-IR data of CO adsorption to the catalysts. Thus, the Pt atom for an AuPt alloy with ∼75% Au would be practically surrounded by Au atoms. Scheme 1 illustrates the proposed reaction pathway for the conversion of methanol to carbonate ion mediated by a gold-platinum bimetallic catalyst.

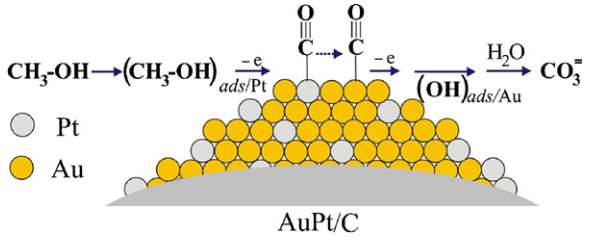

Scheme 1. A schematic illustration of the electrocatalytic oxidation of methanol on AuPt/C catalyst in alkaline electrolyte.

While a detailed delineation of the proposed electrocatalytic mechanism is part of our on-going work, several important insights are supportive of the mechanistic view. The formation of intermediate CO_{ad} species on Pt is a well-known fact. The transfer of the intermediate CO_{ad} species from Pt-atop sites to neighboring Au-atop sites is possible in view of the favorable adsorption of CO on Au nanoparticles known from both experimental measurements [1] and theoretical calculations [17,34]. The formation of Au-OH_{ad} or surface oxides on gold in alkaline electrolyte was in fact proposed to explain some of the electrocatalytic properties observed for a gold electrode (e.g., incipient hydrous oxide/adatom mediator model [39]). Our previous in situ measurements of the interfacial mass change accompanying the electrocatalytic oxidation of methanol also indicated the formation of Au oxides (Au_2O_3, AuOH or $Au(OH)_3$) on gold nanoparticle surfaces [40]. The bifunctional activity in the alkaline electrolyte involves the participation of CO and OH adsorption on Au sites in the catalytic reaction of Pt in the alloy via a combination of reaction steps (see Scheme 1), including the adsorption of MeOH on Pt followed by dehydrogenation, the formation of intermediate CO_{ad}/Pt, the transfer of CO_{ad}/Pt to neighboring Au-atop sites forming CO_{ad}/Au, and the reactions of Pt-CO_{ad} + Au-OH_{ad} and Au-CO_{ad} + Au-OH_{ad} towards the final product (CO_3^{2-}).

4. Conclusions

In conclusion, the AuPt nanoparticles have been shown to exhibit bimetallic surface properties. This finding further led to the correlation of the Au-atop and Pt-atop CO bands on the surface of the alloy nanoparticles of a wide range of bimetallic composition with the electronic effect as a result of the d-band shift of Pt in the bimetallic nanocrystals. This finding, together

with previous findings of the nanocrystal core properties [2], has provided the first evidence that both the core and the surface of the gold-platinum nanoparticles exhibit bimetallic alloy properties. The finding of the maximum mass activity for alkaline conditions around the composition of 65–85% Au coincides remarkably with the finding of the composition of ~65% Au for the transition of the band features for CO adsorption, suggesting a synergistic effect of the surface reactivity for Pt atoms surrounded by Au atoms in the alloyed nanocrystal surface. Further quantitative correlation of the findings with theoretical modeling based on density functional theory [17,33,34,41] along with studies of the catalytic or interfacial reactivities, will provide mechanistic details into fundamental questions related to the bimetallic nanoparticles and catalysts.

Acknowledgements

This work was supported in part by the National Science Foundation (CHE 0316322), the Petroleum Research Fund administered by the American Chemical Society (40253-AC5M), and the GROW program of the World Gold Council. We thank Dr. V. Petkov of Central Michigan University for XRD measurements, and Dr. H. R. Naslund of State University of New York at Binghamton for DCP-AES analysis.

References

[1] M. Haruta, Nature 437 (2005) 1098.
[2] J. Luo, M.M. Maye, V. Petkov, N.N. Kariuki, L. Wang, P. Njoki, D. Mott, Y. Lin, C.J. Zhong, Chem. Mater. 17 (2005) 3086.
[3] V. Ponec, G.C. Bond (Eds.), Catalysis by Metals and Alloys, Elsevier, 1995.
[4] C.S. Kim, C. Korzeniewski, Anal. Chem. 69 (1997) 2349.
[5] M.S. Chen, D. Kumar, C.-W. Yi, D.W. Goodman, Science 310 (2005) 291.
[6] C. Mihut, C. Descorme, D. Duprez, M. Amiridis, J. Catal. 212 (2002) 125.
[7] H. Lang, S. Maldonado, K.J. Stevenson, B.D. Chandler, J. Am. Chem. Soc. 126 (2004) 12949.
[8] X.M. Ren, P. Zelenay, S. Thomas, J. Davey, S. Gottesfeld, J. Power Sources 86 (2000) 111.
[9] D. Chu, R. Jiang, Solid State Ionics 148 (2002) 591.
[10] U.A. Paulus, U. Endruschat, G.J. Feldmeyer, T.J. Schmidt, H. Bonnemann, R.J. Behm, J. Catal. 195 (2000) 383.
[11] E. Antolini, Mater. Chem. Phys. 78 (2003) 563.
[12] G.Q. Lu, A. Wieckowski, Curr. Opin. Colliod Interface Sci. 5 (2000) 95.
[13] K. Nishimura, K. Kunimatsu, M. Enyo, J. Electroanal. Chem. 260 (1989) 167.
[14] M. Morita, Y. Iwanaga, Y. Matsuda, Electrochim. Acta 36 (1991) 947.
[15] A.B. Anderson, E. Grantscharova, S. Seong, J. Electrochem. Soc. 143 (1996) 2075.
[16] L.D. Burke, J.A. Collins, M.A. Horgan, L.M. Hurley, A.P. O'Mullane, Electrochim. Acta 45 (2000) 4127.
[17] M.Ø. Pedersen, S. Helveg, A. Ruban, I. Stensgaard, E. Lægsgaard, J.K. Nørskov, F. Besenbacher, Surf. Sci. 426 (1999) 395.
[18] J.W.A. Sachtler, G.A. Somorjai, J. Catal. 81 (1983) 77.
[19] J. Luo, M.M. Maye, N.N. Kariuki, L. Wang, P. Njoki, Y. Lin, M. Schadt, H.R. Naslund, C.J. Zhong, Catal. Today 99 (2005) 291.
[20] J. Luo, V.W. Jones, M.M. Maye, L. Han, N.N. Kariuki, C.J. Zhong, J. Am. Chem. Soc. 124 (2002) 13988.
[21] J. Luo, P. Njoki, Y. Lin, L. Wang, D. Mott, C.J. Zhong, Electrochem. Comm. 8 (2006) 581.
[22] J. Luo, P. Njoki, Y. Lin, D. Mott, L. Wang, C.J. Zhong, Langmuir 22 (2006) 2892.
[23] M. Brust, M. Walker, D. Bethell, D.J. Schiffrin, R.J. Whyman, Chem. Soc. Chem. Commun. (1994) 801.
[24] M.J. Hostetler, C.J. Zhong, B.K.H. Yen, J. Anderegg, S.M. Gross, N.D. Evans, M.D. Porter, R.W. Murray, J. Am. Chem. Soc. 120 (1998) 9396.
[25] J. Luo, M.M. Maye, L. Han, N. Kariuki, V.W. Jones, Y. Lin, M.H. Engelhard, C.J. Zhong, Langmuir 20 (2004) 4254.
[26] P.N. Njoki, J. Luo, L. Wang, M.M. Maye, H. Quaizar, C.J. Zhong, Langmuir 21 (2005) 1623.
[27] D. Mott, J. Luo, A. Smith, P.N. Njoki, L. Wang, C.J. Zhong, Nanoscale Res. Lett. 2 (2007) 12.
[28] P.J. Hsu, S.K. Lai, J. Chem. Phys. 124 (2006) 44711.
[29] D.C. Meier, D.W. Goodman, J. Am. Chem. Soc. 126 (2004) 1892.
[30] J.E. Bailie, G.J. Hutchings, Chem. Commun. (1999) 2151.
[31] R. Meyer, C. Lemire, Sh.K. Shaikhutdinov, H.-J. Freund, Gold Bull. 37 (2004) 72.
[32] J.C. Vickerman (Ed.), Surface Analysis: The Principle Techniques, John Wiley & Sons, 1997.
[33] Q. Ge, C. Song, L. Wang, Compos. Mater. Sci. 35 (2006) 247.
[34] C. Song, Q. Ge, L. Wang, J. Phys. Chem. B 109 (2005) 22341.
[35] T. Page, R. Johnson, J. Hormes, S. Noding, B. Rambabu, J. Electroanal. Chem. 485 (2000) 34.
[36] C. Berg, H.J. Venvik, F. Strisland, A. Ramstad, A. Borg, Surf. Sci. 409 (1998) 1.
[37] M. Haruta, Catal. Today 36 (1997) 153.
[38] M. Haruta, M. Date, Appl. Catal. A 222 (2001) 427.
[39] L.D. Burke, Gold Bull. 37 (2004) 125.
[40] J. Luo, M.M. Maye, L. Han, C.J. Zhong, M. Hepel, J. New Mater. Electrochem. Syst. 5 (2000) 237.
[41] G.F. Wang, M.A. Van Hove, P.N. Ross, M.I. Baskes, Prog. Surf. Sci. 79 (2005) 28.